Eleventh Workshop
"Solar influences on the magnetosphere, ionosphere a nd atmosphere"
Primorsko, Bulgaria, 3 ÷ 7 June 2019

Comparing the Height Dependences of the Magnetic Field Overlying the Initial Areas of Fast and Slow Coronal Mass Ejections

Zagainova Iuliia[1], Fainshtein Viktor[2], Rudenko George[2]

1 - Pushkov Institute of Terrestrial Magnetism, Ion osphere and Radio Wave Propagation Russian Academy of Sciences, Russian Federation

2 - Institute of solar-terrestrial physics, Russian Federation

CME kinematic properties

JOURNAL OF GEOPHYSICAL RESEARCH, VOL. 104, NO. A11, PAGES 24,739–24,767, NOVEMBER 1, 1999

Continuous tracking of coronal outflows: Two kinds of coronal mass ejections

N. R. Sheeley Jr., J. H. Walters,[1] Y.-M. Wang, and R. A. Howard

E. O. Hulburt Center for Space Research, Naval Research Laboratory, Washington, D. C.

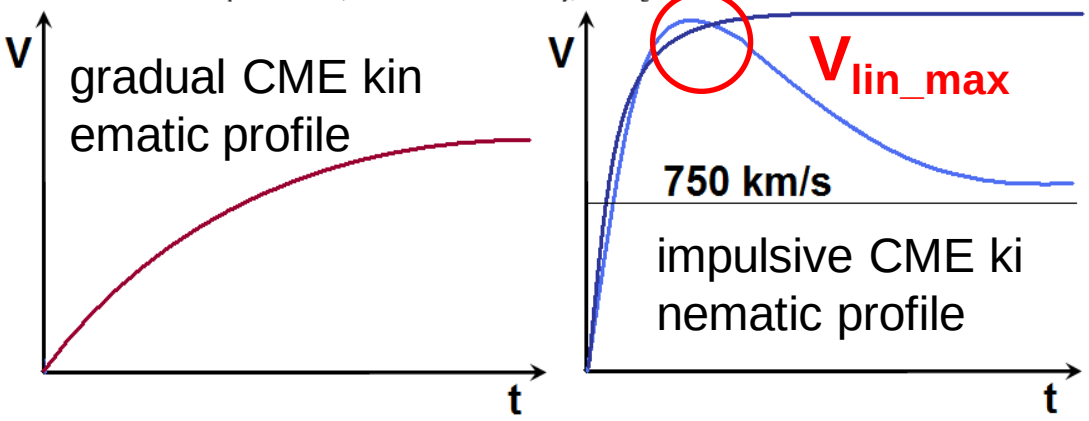

Coronal mass ejections (CMEs) are characterized by a wide range of maximum velocities V_{lin_max} in the coronagraph field-of-view (FOV)

V_{lin_max} vary greatly from N*10 to ~3000 km/sec… (***Gopalswamy et al, 2009***).

Fast CMEs: $V_{lin\_max} > 1300$ km/sec

Intermediate CMEs: $600 < V_{lin\_max} \leq 1300$ km/sec;

Slow CMEs: $V_{lin\_max} \leq 600$ km/sec;

We studied halo CMEs associated with eruptive phenomena or low coronal signatures (LCSs) in the lower corona such as solar flares, filament eruptions, extreme ultraviolet (EUV) waves, magnetic reconfiguration, or jets.

What is the maximum of the $V_{KBM}(t)$?

Astron. Nachr. / AN 328, No. 8, 743 – 746 (2007) / DOI 10.1002/asna.200710795

Numerical simulations of fast and slow coronal mass ejections

T. Török[1,*] and B. Kliem[2,3]

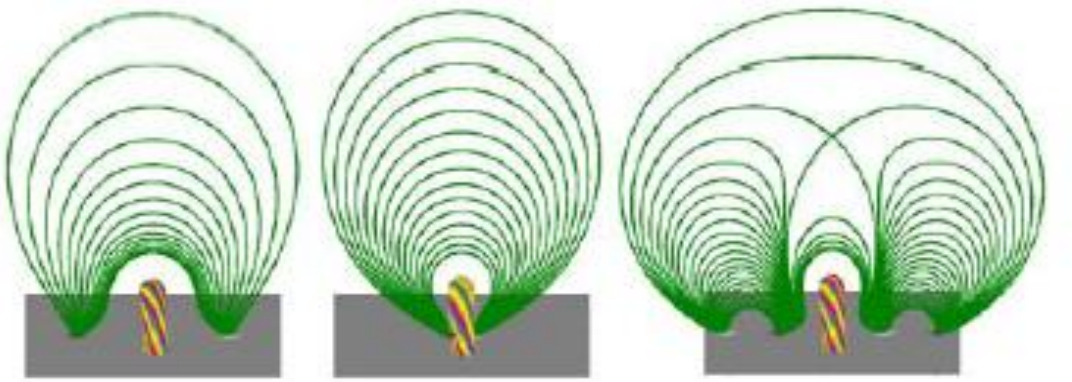

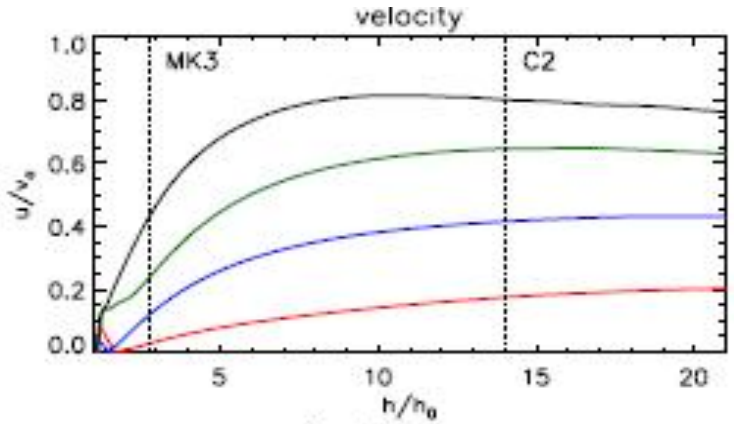

Velocities are normalized to the initial Alfvén velocity v_a at the flux rope apex $\tau_a = h_0/v_a$.
The quadrupolar configuration yields the most impulsive acceleration and the highest terminal velocity.

Acceleration profile of the magnetic flux-rope is defined by radial gradient of the magnetic field -

Decay index $D_i = -\frac{dB}{dr} \cdot \frac{r}{B}$

Authors suggested if the magnetic field decreases with height quickly than Fast CME is formed, in any cases CME should be Slow one.

And what is it really?

Data

CMEs-list: https://cdaw.gsfc.nasa.gov/CME_list/index.html

HCMEs-list: https://cdaw.gsfc.nasa.gov/CME_list/HALO/index.html

Rudenko G. V., Anfinogentov S. A. Very Fast and Accurate Azimuth Disambiguation of Vector Magnetograms // Solar Physics. V. 289. Issue 5. PP. 1499-1516. 2014.

SDO AIA and HMI: http://jsoc.stanford.edu/ajax/exportdata.html

Solar active monitor: https://solarmonitor.org/

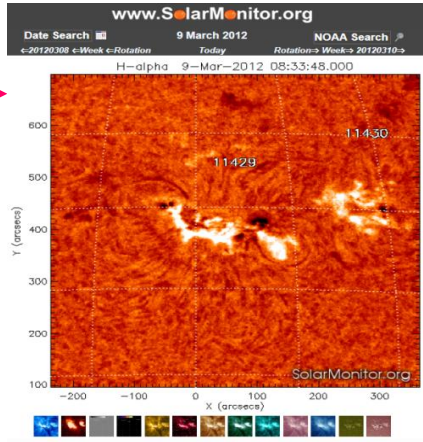

For our studies we selected 26 events: 9 Slow halo coronal mass ejection (HCME), 9 Intermediate HCMEs and 8 Fast HCMEs with source areas close to the solar disk center.

Fast HCMEs (V_{lin_max} > 1300 km/sec)

First C2 Appearance Date Time [UT]		Linear Speed [km/s]	Space Speed [km/s]	Accel [m/s2]	MPA [deg]	CME Source Location	X-ray Importance	Flare onset	AR of CME Source Location	Flare Source Location	AR Center Location
2011/08/04	04:12:05	1315	1477	-41.1	298	N19W36	M9.3	03:41	11261	N16W51	(710"; 190")
2012/01/23	04:00:05	2175	2511	28.0	326	N28W21	M8.7	03:38	11405	N12W27	(422"; 96")
2012/03/07	00:24:06	2684	3146	-88.2	57	N17E27	X5.4	00:02	11429	N17E15	(-235"; 169")
2012/03/07	01:30:24	1825	2160	-160.9	82	N15E26	X1.3	01:05	11429	N17E15	(-235"; 169")
2014/01/07	18:24:05	1830	2246	-60.8	231	S15W11	X1.2	18:04	11944	S09W01	(16"; -89")
2015/06/18	17:24:24	1305	1398	-23.7	92	N15E50	M3.0	16:30	12371	N12E39	(-583"; 178")
2015/06/21	02:36:05	1366	1740	21.2*1	72	N12E16	M2.6	02:06	12371	N12E39	(-90"; 185")
2015/06/25	08:36:05	1627	1805	-24.8	330	N09W42	M7.9	08:02	12371	N11W45	(656"; 155")

SOHO LASCO CME CATALOG: https://cdaw.gsfc.nasa.gov/CME_list/UNIVERSAL/2017_01/univ2017_01.html

SOHO/LASCO HALO CME CATALOG:
https://cdaw.gsfc.nasa.gov/CME_list/halo/halo.html

Intermediate HCMEs ($600 < V_{lin\_max} \leq 1300$ km/sec)

First C2 Appearance Date Time [UT]		Linear Speed [km/s]	Space Speed [km/s]	Accel [m/s2]	MPA [deg]	CME Source Location	X-ray Importance	Flare onset	AR of CME Source Location	Flare Source Location	AR Center Location
2011/02/15	02:24:05	669	960	-18.3	189	S20W12	X2.2	01:44	11158	S21W28	(417"; -433")
2011/06/21	03:16:10	719	882	-1.3	65	N16W08	C7.7	01:22	11236	N17W21	(326"; 173")
2011/09/06	02:24:05	782	1232	105.6*1	70	N14W07	M5.3	01:35	11283	N14W18	(285"; 122")
2012/01/19	14:36:05	1120	1269	54.1	20	N32E22	M3.2	13:44	11402	N28E13	(-189"; 344")
2012/03/09	04:26:09	950	1229	-13.5*1	29	N15W03	M6.3	03:22	11429	N17W13	(204"; 169")
2012/03/10	18:00:05	1296	1638	-10.9	5	N17W24	M8.4	17:15	11429	N18W27	(411"; 194")
2013/10/28	15:36:05	812	1098	-17.7	86	S06E28	M4.4	15:07	11882	S08E21	(-344"; -207")
2014/12/19	01:04:42	1195	1513	-57.0	98	S11E15	M6.9	21:41	12241	S09W09	(151"; -128")
2015/12/28	12:12:05	1212	1471	4.6*1	163	S23W11	M1.8	11:20	12473	S22W18	(280"; -327")

SOHO LASCO CME CATALOG: https://cdaw.gsfc.nasa.gov/CME_list/UNIVERSAL/2017_01/univ2017_01.html

SOHO/LASCO HALO CME CATALOG:
https://cdaw.gsfc.nasa.gov/CME_list/halo/halo.html

Slow HCMEs ($V_{lin\_max} \leq 600$ km/sec)

First C2 Appearance Date	Time [UT]	Linear Speed [km/s]	Space Speed [km/s]	Accel [m/s2]	MPA [deg]	CME Source Location	X-ray Importance	Flare onset	AR of CME Source Location	Flare Source Location	AR Center Location
2012/04/23	18:24:05	528	769	-1.1*1	234	N14W17	C2.0	17:38	11461	N15W23	(250"; 84")
2012/11/21	16:00:05	529	942	-9.4*1	194	N05E05	M3.5	15:10	11618	N08W00	(0"; 17")
2013/10/22	21:48:06	459	1070	-10.1*1	190	N04W01	M4.2	21:15	11875	N06E05	(-83"; 13")
2013/11/07	15:12:10	411	626	-4.9*1	130	S13E23	M2.4	14:15	11890	S11E10	(-165"; -244")
2014/02/12	06:00:05	373	725	7.3*1	328	S12W02	M3.7	03:52	11974	S12W11	(182"; -91")
2014/03/29	18:12:05	528	679	-4.1	325	N11W32	X1.0	17:35	12017	N10W32	(503"; 259")
2014/04/29	23:24:05	553	833	-18.3*1	180	S12E15	B9.1	22:28	12047	S18E14	(-220"; -228")
2014/12/17	05:00:05	587	855	-2.1	162	S20E09	M8.7	04:25	12242	S19W02	(32"; -298")
2015/04/18	15:12:08	428	745	11.1*1	333	N10W15	C5.2	14:03	12321	N11W22	(352"; 263")

SOHO LASCO CME CATALOG: https://cdaw.gsfc.nasa.gov/CME_list/UNIVERSAL/2017_01/univ2017_01.html

SOHO/LASCO HALO CME CATALOG:
https://cdaw.gsfc.nasa.gov/CME_list/halo/halo.html

Methods

Over the recent years, 3D reconstruction of the coronal magnetic field using the non-linear force-free approximation (NLFFF) has become a standard tool, see, for example (Wheatland et al., 2000); Wiegelmann, 2004).

The most commonly used algorithm of the NLFFF reconstruction is the optimization method (Wheatland et al., 2000; Wiegelmann, 2004) and its extended version (Wiegelmann et al., 2006) that includes preprocessing of the photospheric magnetograms.

The spatial distribution of the magnetic field over the active region where the eruptive event occurred was calculated in the NLFFF modeling. The force free condition is defined:

$$\nabla \times B = a(x, y, z)$$

where a is a scalar value function referred to as a force-free parameter. The force-free approximation is applicable to the weakly varying coronal magnetic field since the plasma β parameter is known to be very low in the solar corona.

Such calculations rely on distributions of the full photospheric magnetic vector. Within the NLFFF approximation, the electric current is always parallel to the magnetic field vector.

Methods

In our study we use an implementation of the optimization method proposed by (Rudenko and Myshyakov, 2009). This technique uses a complete set of the evolutionary field equations (see Appendix Wheatland, Sturrock, and Roumeliotis (2000)), including those at the boundary of the calculated region, except for the photosphere.

G.V. Rudenko · I.I. Myshyakov Solar Phys (2009) 257: 287–304

Analysis of Reconstruction Methods for Nonlinear Force-Free Fields

In this year Rudenko G. optimized the NLFFF method (Wheatland et al., 2000).

We use the SDO/HMI measurements of the photospheric magnetic field vector as the boundary conditions for our NLFFF reconstructions by Rudenko Gorge.

Formation stage of the intermediate HCME frontal structure

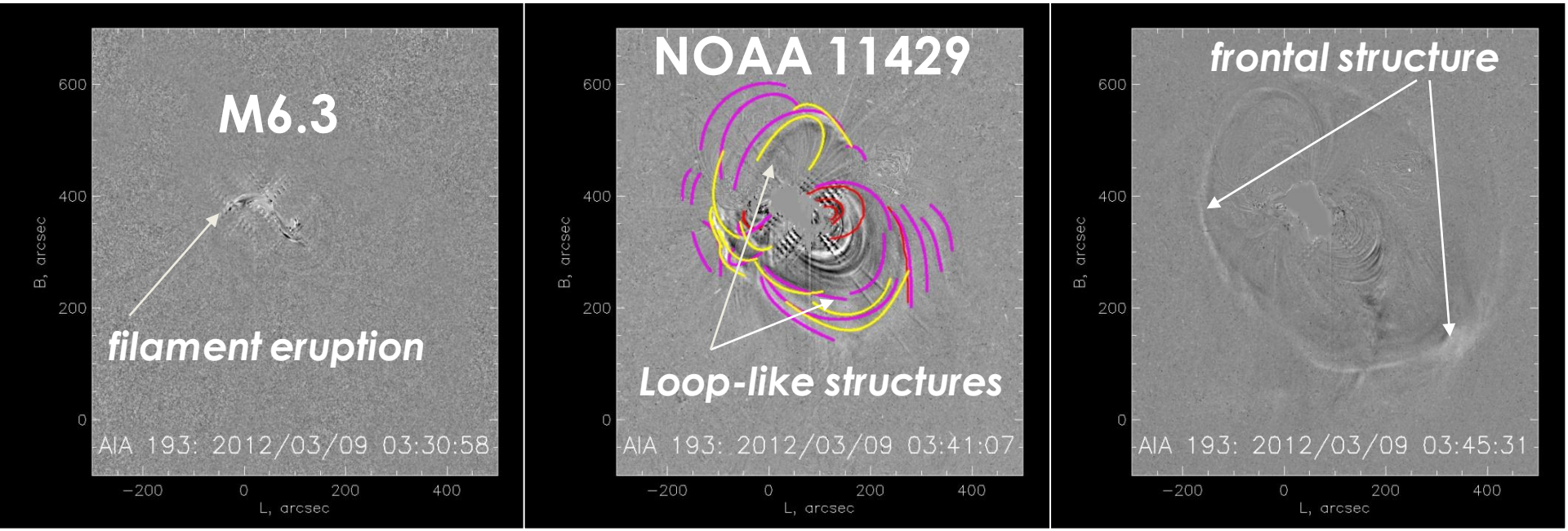

Before the initiation stage of Intermediate HCME the filament eruption starting was observed at 03:45 UT. After 10 minutes many different loop-like structures were detected. Later than 03:45 UT the HCME frontal structure was observed.

Active Region NOAA 11429 on 2012, March 9 wit h the source region of the intermediate HCME

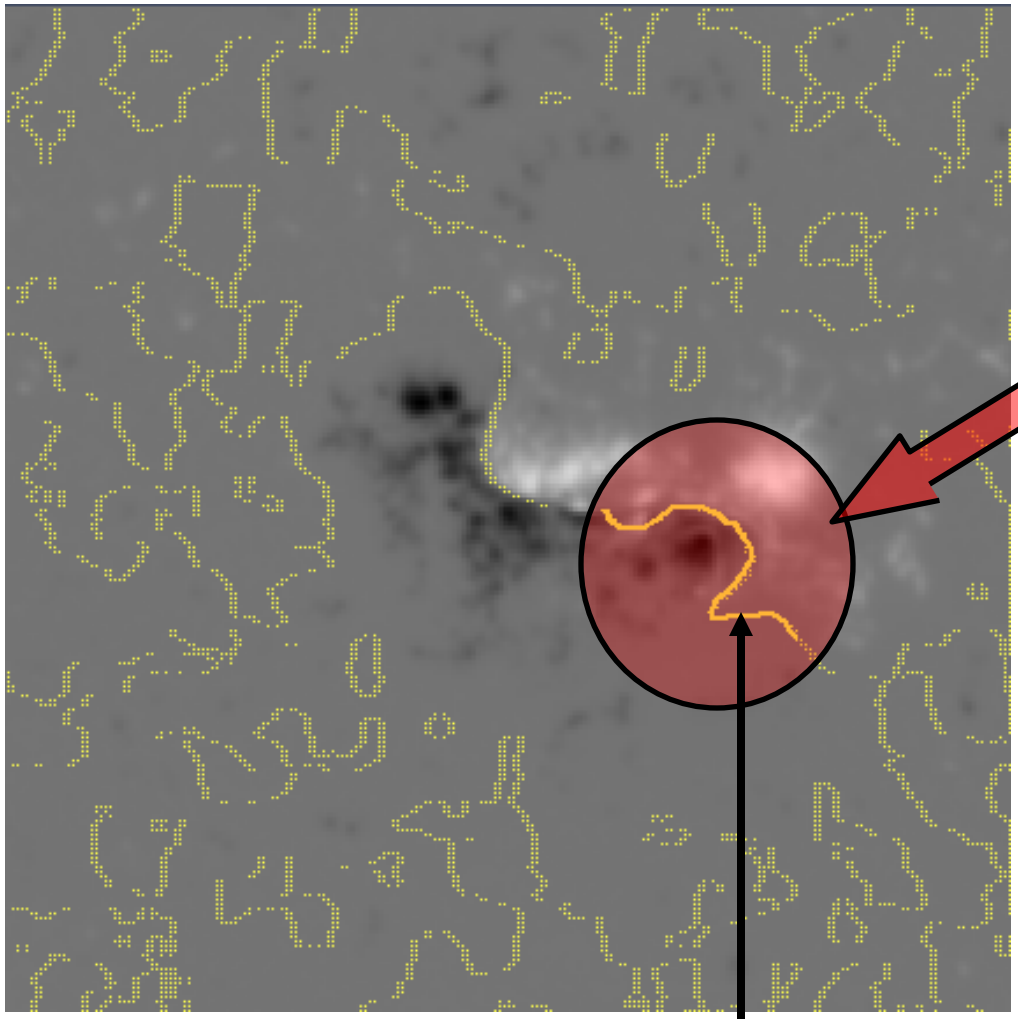

Source area location of the coronal mass ejection

Yellow-colored line mark the polarity inversion line on the photospheric magnetogram (L_{PIL})

2D Decay-index variations with altitude before X-ray flare onset (~ 1 hour)

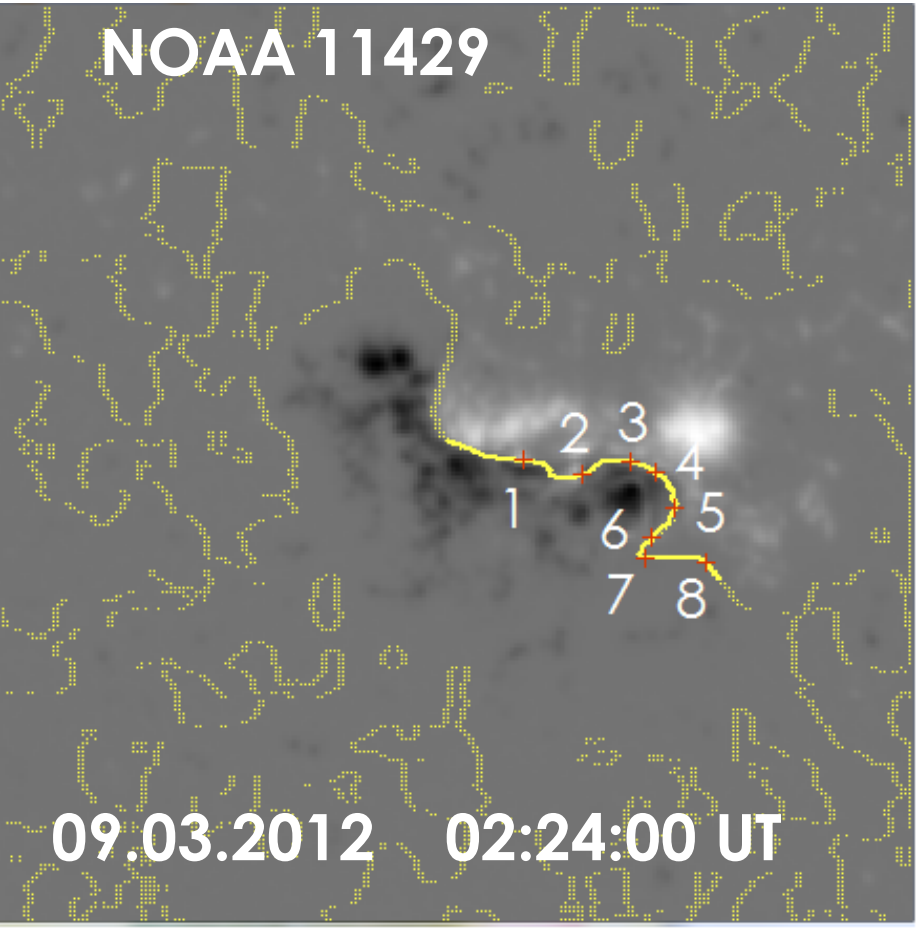

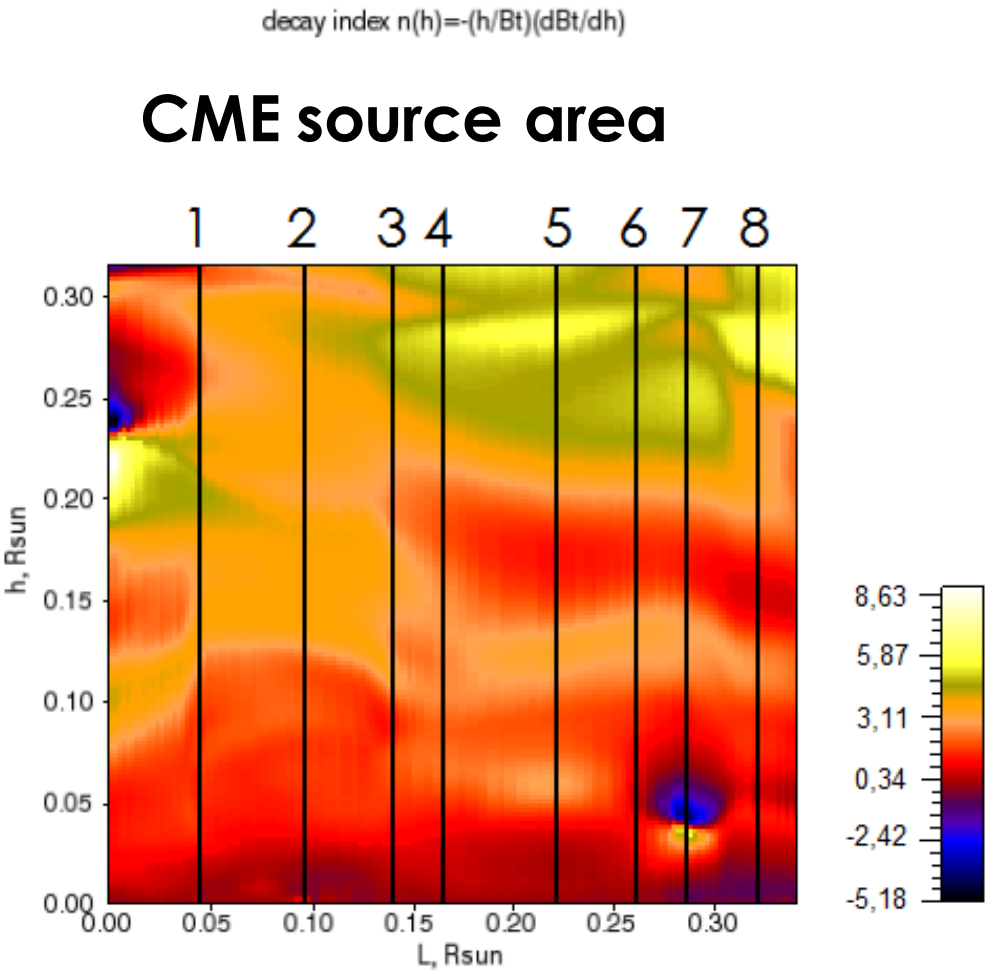

Di-variations with altitude at different locations of the polarity inversion line (PIL)

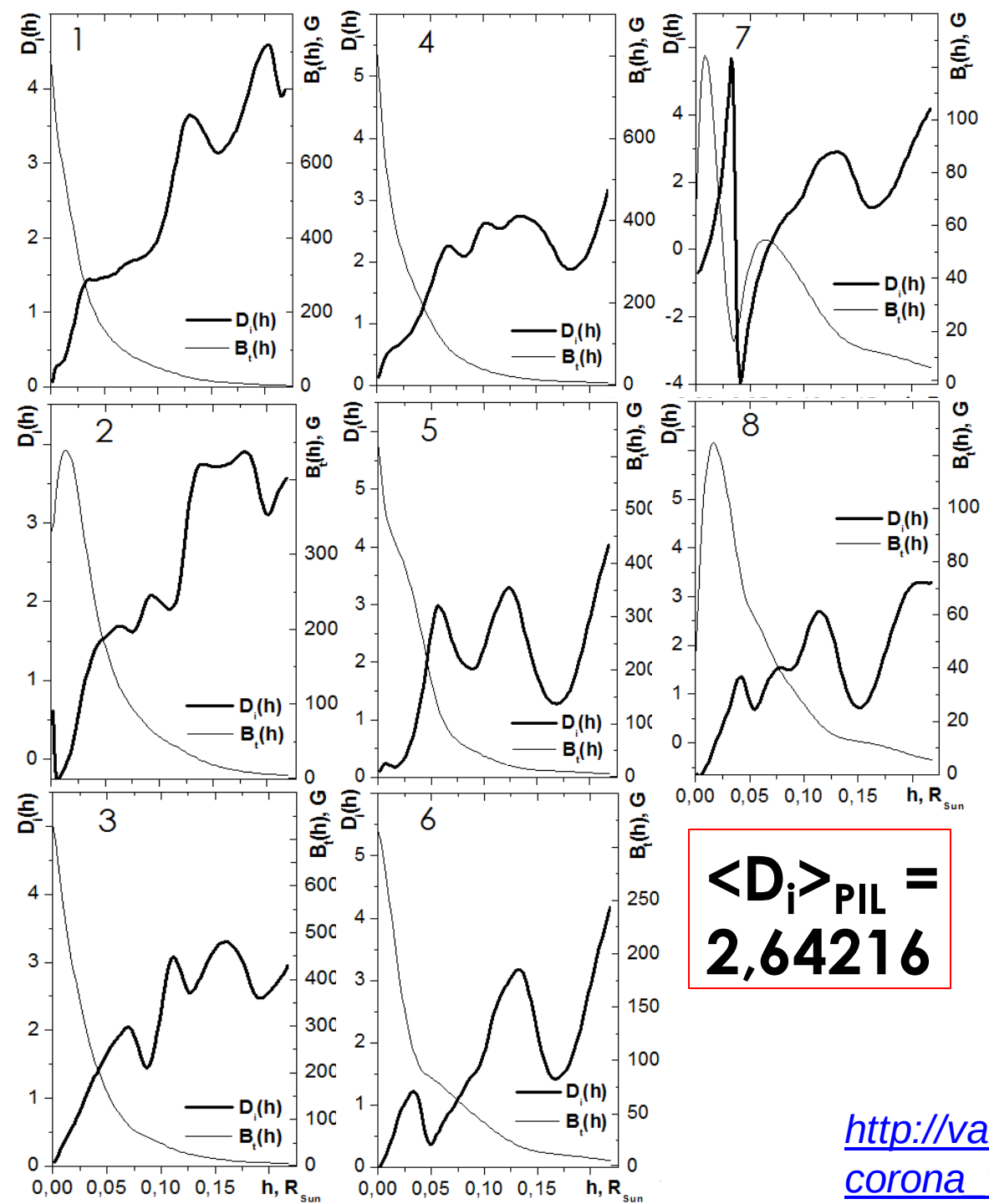

$\langle D_i \rangle_{PIL} = 2{,}64216$

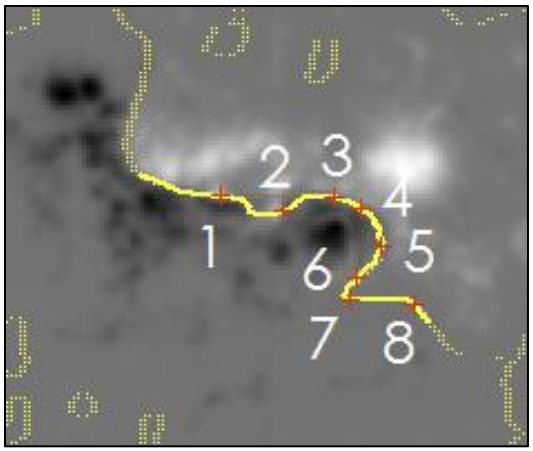

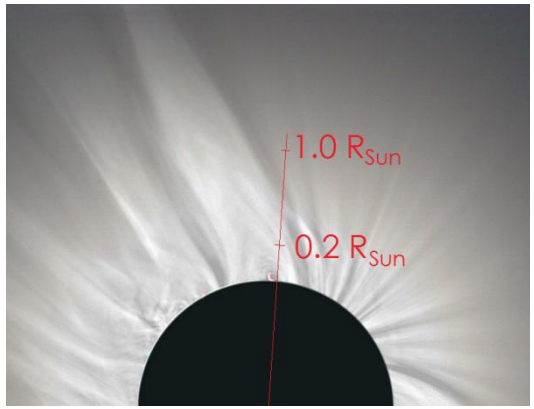

http://variable-stars.ru/db/msg/1235651/corona_vangorp_big.jpg.html

The dependence of the mean Decay_index before 1 hour of a flare onset on the HCME maximum velocity V_{lin_max} in the LASCO C2 FOV

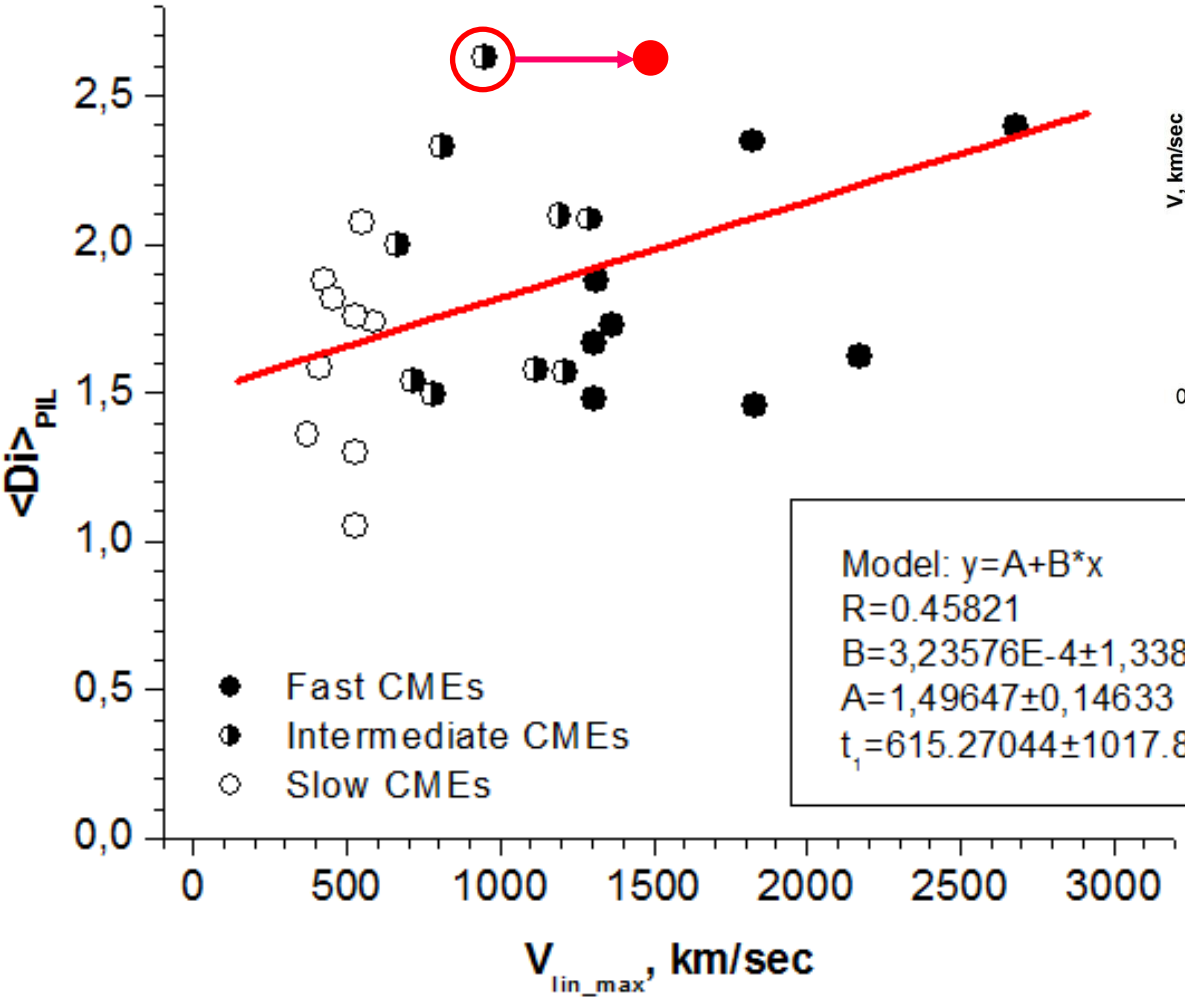

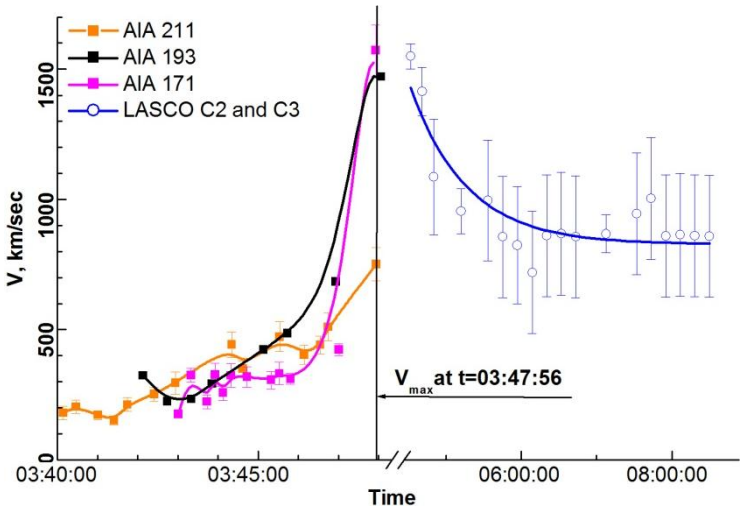

SOHO/C2:

V_{lin_max}=**950** km/sec at 04:26:09 UT

SDO/AIA:

V_{FS}~ **1500** km/sec

Conclusions

1. Maximum velocities of HCMEs depend on the altitude radial gradient of the tangential component of magnetic field before a flare onset.

2. We have found that from $h=0.25\ R_{Sun}$ to $h=0.25\ R_{sun}$ the $\mathbf{<D_i>}$ of the tangential component of the magnetic field above the polarity inversion line in Slow HCMEs source areas was at least 30 per cent lower than the $\mathbf{<D_i>}$ values for Fast HCMEs.